

Multi-Wound Axial Flux Generators with Halbach Array Rotors

Matin Vatani

SPARK Lab, Pigman Eng. College
University of Kentucky
Lexington, KY, USA
matin.vatani@uky.edu

Yaser Chulaee

SPARK Lab, Pigman Eng. College
University of Kentucky
Lexington, KY, USA
yaser.chulaee@uky.edu

John F. Eastham

Dept. of Electronic & Electrical Eng.
University of Bath
Claverton Down, Bath, UK
jfeastham@aol.com

Xiaoze Pei

Dept. of Electronic & Electrical Eng.
University of Bath
Claverton Down, Bath, UK
X.Pei@bath.ac.uk

Dan M. Ionel

SPARK Lab, Pigman Eng. College
University of Kentucky
Lexington, KY, USA
dan.ionel@ieee.org

Abstract—This paper presents three coreless axial flux permanent magnet (AFPM) generator topologies that feature magnetically and electrically decoupled outputs using a single prime mover. The proposed topologies include: (1) two separate generators mounted on the same shaft, (2) a nested configuration with a smaller generator inside a larger one, and (3) a multi-wound generator with two sets of windings and different pole numbers for each rotor side. The multi-wound generator is selected for further investigation due to its superior power-to-volume ratio and the advantage of utilizing a single structure for stator cooling. The airgap magnetic flux density equation is derived using the superposition technique to analytically explore the effects of rotor pole number differences. Additionally, three-dimensional finite element analysis (FEA) is employed to investigate the magnetic cross-coupling between different stators.

Index Terms—Multi-wound generator, axial flux PM machine, coreless stator, Halbach array, 3D FEA, analytical modeling.

I. INTRODUCTION

The size and volume of the electric propulsion system are crucial factors for electric transport, such as road vehicles, ships, and airplanes. For example, a hybrid electric vehicle requires at least two separate generators: one for internal functions like lighting and another to charge the battery and power the propulsion system. Each generator necessitates its own mechanical connections and prime mover, which increases the overall size and mass of the system [1].

A solution to improve the system's compactness is to use dual or multi-wound generators, which feature segregated windings on a single generator driven by one prime mover. This type of generator has multiple windings that share a stator, each winding corresponding to different rotor pole numbers. These different pole numbers can be achieved through wound rotors that produce different polarities or PM-excited rotors with complex designs. Therefore, this topology allows different loads to be powered by a single prime mover. Examples of such generators can be found in [1–3].

Since each of the stator windings within the multi-wound generator topology feeds separate loads, they must be electrically and magnetically decoupled. While electrical decoupling is straightforward, eliminating magnetic cross-coupling between windings requires precise winding design. Additionally, each of the two stator windings should only magnetically couple with its designated rotor's pole number. Various stator winding strategies applicable to dual-wound machines are detailed in [4].

While radial flux machines with dual stator windings have been extensively studied, there is a gap in the literature on multi-wound axial flux machines. This paper proposes three different topologies of axial flux permanent magnet (AFPM) machines with coreless stators that utilize a single prime mover to feed separate loads, resulting in more compact electromagnetic and mechanical structures.

Axial flux PM machines are recognized for their high aspect-ratio planar structures, compact design, and relatively high torque density [5, 6]. Moreover, the axial flux topology allows for the integration of multiple units on a single shaft, offering greater compactness than radial flux counterparts, as the two sets of end windings in radial flux machines create volumetric overhead in the central area.

Among various AFPM machine configurations, the coreless (air-cored) type offers unique advantages, such as low starting torque, minimal vibration, potentially high efficiency, and high-power density [7–9]. Because the windings are not confined to stator slots, stator cooling can be more straightforward. The absence of a magnetic core also creates an opportunity to utilize printed circuit board (PCB) stators, which provide flexibility in coil design and offer potentially reliable and repeatable fabrication [10, 11].

Axial flux PM machines commonly employ a surface-mounted PM rotor that features an alternating polarity arrangement of permanent magnets and a back iron that serves as a return flux path. An alternative to this configuration is the

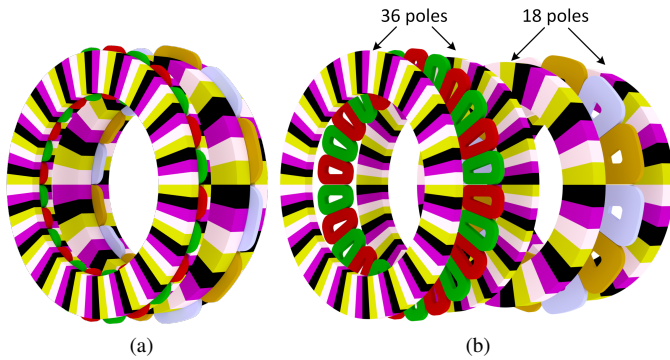


Fig. 1. Two coreless AFPM generators with double-sided Halbach array rotors topology mounted on a single shaft, delivering electrically and magnetically decoupled two-phase outputs.

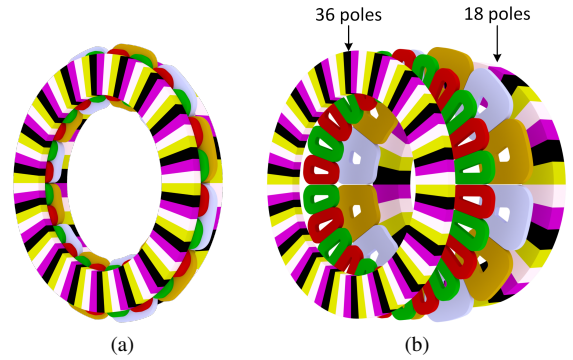


Fig. 3. Proposed coreless AFPM generator featuring different pole numbers for each rotor side and two electrically and magnetically decoupled stators within the shared air gap, each corresponding to one of the rotors.

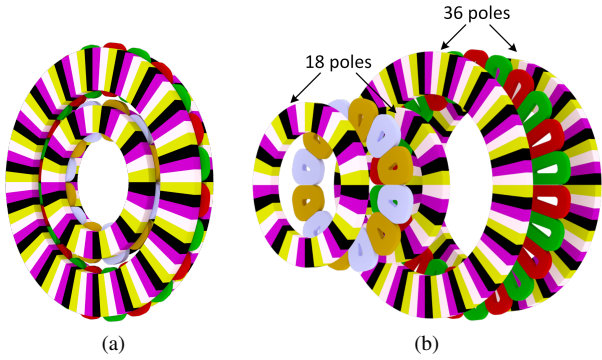


Fig. 2. Two generators with different outer diameters, with the smaller one nested inside the larger one, both mounted on a single shaft. The smaller generator provides significantly lower power, but the overall structure is more compact compared to the previous design.

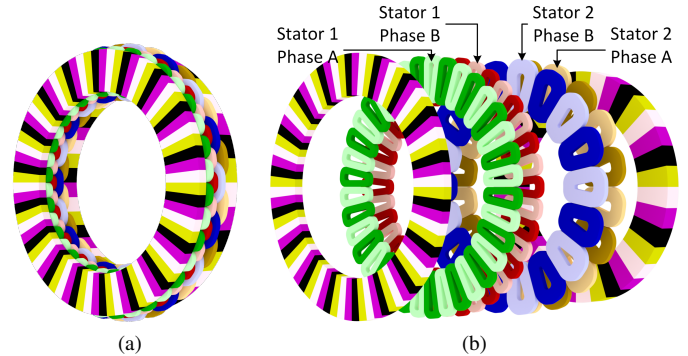


Fig. 4. Coreless AFPM generator with a double-sided Halbach array rotor of different polarities and a two-layer overlapping winding configuration. Each layer of coils corresponds to one phase and one stator. In each phase, current is injected into the brightly colored coils in the opposite direction of the solid-colored coils.

Halbach array magnetization, which creates a strong magnetic field on one side of the rotor while producing a nearly zero field on the opposite side [12, 13]. This rotor configuration has been gaining popularity due to its ability to generate up to 40% more torque within a similar rotor envelope than traditional surface-mounted PM rotors.

The structure of the paper is organized as follows: Section II introduces the proposed multi-output coreless AFPM generators. Section III develops the equations for magnetic flux density and presents the analytical modeling of the magnetic field. Section IV covers the three-dimensional finite element analysis (FEA) of the third proposed generator concept. Section V addresses cooling, and the eddy current losses associated with this generator concept, and Section VI provides the conclusion.

II. MULTI-OUTPUT CORELESS AFPM GENERATOR TOPOLOGIES

This paper presents three different coreless AFPM generator topologies to achieve multiple electrically and magnetically isolated outputs for separate loads, as depicted in Figs. 1, 2, and 3. Each topology features Halbach PM array rotors with four magnets per wavelength, and these rotors can have either identical or different pole numbers. The stators consist

of concentrated coils arranged in a span of four coils over six poles, each providing a two-phase output. The two-phase winding configuration was chosen due to the zero coupling between phases, which are separated by 270 electrical degrees. This design choice enhances reliability by minimizing the impact of faults from one phase to another.

The first topology, illustrated in Fig. 1, comprises two separate coreless AFPM generators mounted on a single shaft, each supplying a two-phase output. Given that all topologies have the same outer diameter, this configuration is the least compact due to its greater axial length, and it is likely the most expensive option because it requires four Halbach array rotors. However, this topology offers the highest level of reliability due to its redundancy.

In the second topology, one generator from the first design has its outer diameter reduced so that it can nest within the bore area of the other generator, as shown in Fig. 2. This configuration is considerably more compact than the first topology. However, the overall power output from both generators combined is significantly lower.

The average torque for a two-phase coreless AFPM machine

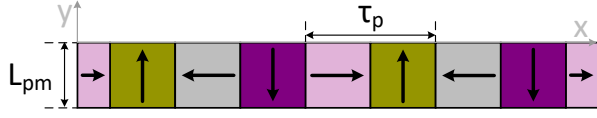


Fig. 5. The unrolled 2D model of a single-sided axial Halbach array rotor, featuring different pole numbers, displayed for two wavelengths.

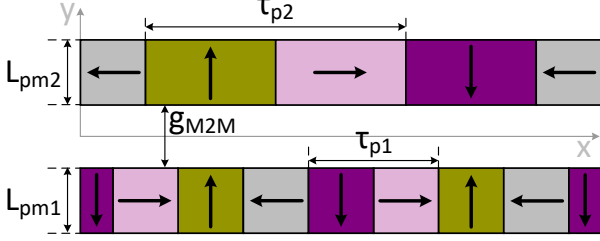


Fig. 6. The unrolled 2D model of a double-sided axial Halbach array rotor, featuring different pole numbers on each side. In this example, the lower rotor has twice the number of poles as the upper rotor.

with a coil span of three coils over four poles is expressed as:

$$T_{avg} = K_1 N I_p k_w B_n P D_{ro}^2 \frac{\lambda^2 - 1}{\lambda^2}, \quad (1)$$

where K_1 is a constant with a value of $\frac{1}{6}$, I_p denotes the peak current, k_w represents the total winding factor, B_n is the peak flux density, D_{ro} is the outer diameter of the rotor, and λ is the ratio of the rotor's outer diameter to its inner diameter, given by $\lambda = \frac{D_{ro}}{D_{ri}}$. The term P signifies the number of poles.

It is shown in [13] that the optimum value for the Halbach PM rotor radial length is given by $\frac{D_{ro} - D_{ri}}{2\tau_p} = 1$. By adjusting this ratio, the optimal value for λ can be calculated as:

$$\frac{D_{ro} - D_{ri}}{2\tau_p} = 1 \xrightarrow{\lambda = \frac{D_{ro}}{D_{ri}}} \lambda = \frac{P + \pi}{P - \pi} \quad (2)$$

For the example design shown in Fig. 2, the larger generator has 36 poles and the smaller generator has 18 poles. Assuming that the outer diameter of the smaller generator is 70% of that of the larger generator and substituting these ratios into equations (1) and (2) indicates that the power output of the smaller generator will be 35% of that of the larger one.

The third topology, depicted in Fig. 3, employs a double-sided Halbach array rotor with different polarities on each side. Two stators share the air gap, each corresponding to one side of the rotor. This configuration allows for an integrated mechanical and cooling structure of the stator, further reducing the generator's mass and volume. In principle, more than two stator windings can be accommodated as long as the rotor polarities are appropriately selected.

This third topology is potentially more compact and has a higher specific power density compared to the first and second configurations. As demonstrated in the subsequent sections, despite the close proximity of the two stators within the same magnetic air gap, the magnetic coupling between them can be eliminated.

For all the proposed generator topologies, an overlapping

winding configuration with a potentially higher winding factor can be employed instead of a concentrated structure. An example design of this winding structure is shown in Fig. 4 for the third topology, where each stator consists of two layers of coils, with each layer dedicated to one phase. Each coil spans 180 electrical degrees, and the current in two adjacent coils differs by 180 electrical degrees.

The overlapping winding configuration performs better for coreless AFPM generators in the first and second topologies because the phases of one stator have a similar distance from the rotor surfaces, producing uniform back-EMF values. In the third topology, however, the inner phase of each stator is farther from the rotor surface compared to the outer stator, resulting in higher back-EMF levels for phases closer to the rotor surfaces.

The performance characteristics of the first and second topologies mirror those of a double-sided coreless AFPM machine, as presented in multiple references, including [13, 14]. However, the electromagnetic performance of the third topology, which features double-sided Halbach array rotors with different polarities, remains unexplored. Therefore, this paper aims to develop an analytical method for calculating the magnetic flux density produced by these Halbach array rotors and to evaluate the electromagnetic performance of this innovative topology.

III. MAGNETIC FIELD ANALYSIS

This section develops the magnetic flux density equations for double-sided Halbach array rotors with varying pole numbers. These equations are formulated by superimposing the flux densities of two single-sided Halbach array rotors. They can subsequently be utilized to assess the power output of the machine through the Lorentz force equation.

The two-dimensional flux density equation for two Halbach array rotors that face each other and have the same pole number has been derived by solving Poisson equations and applying Fourier transforms as demonstrated in [15, 16]. By employing the same methodology and performing some modifications and manipulations, a similar equation can be obtained for a single-sided Halbach array as:

$$B_y = B_r \sum_{i=0}^{\infty} \frac{\sin(\epsilon n \pi / m)}{n \pi / m} \left[1 - \exp\left(\frac{-n \pi L_{pm}}{\tau_p}\right) \right] \exp\left(\frac{-n \pi y}{\tau_p}\right) \sin\left(\frac{n \pi x}{\tau_p}\right), \quad (3)$$

where ϵ usually set to one, $n = 1 + mi$, and m is the number of PMs per wavelength, B_r is the remanence of the PMs, L_{pm} is the PM length, $\tau_p = \frac{\pi D_{avg}}{P}$ is the pole pitch, D_{avg} is average diameter, P is the pole number, and x and y are the positions regarding the x and y axis defined in Fig. 5.

By applying the superposition principle and utilizing (3) for two different pole numbers, the resultant flux density for a double-sided Halbach array rotor with varying pole numbers on each side can be determined from 4, shown at the bottom of the page. An example illustrating this scenario is depicted

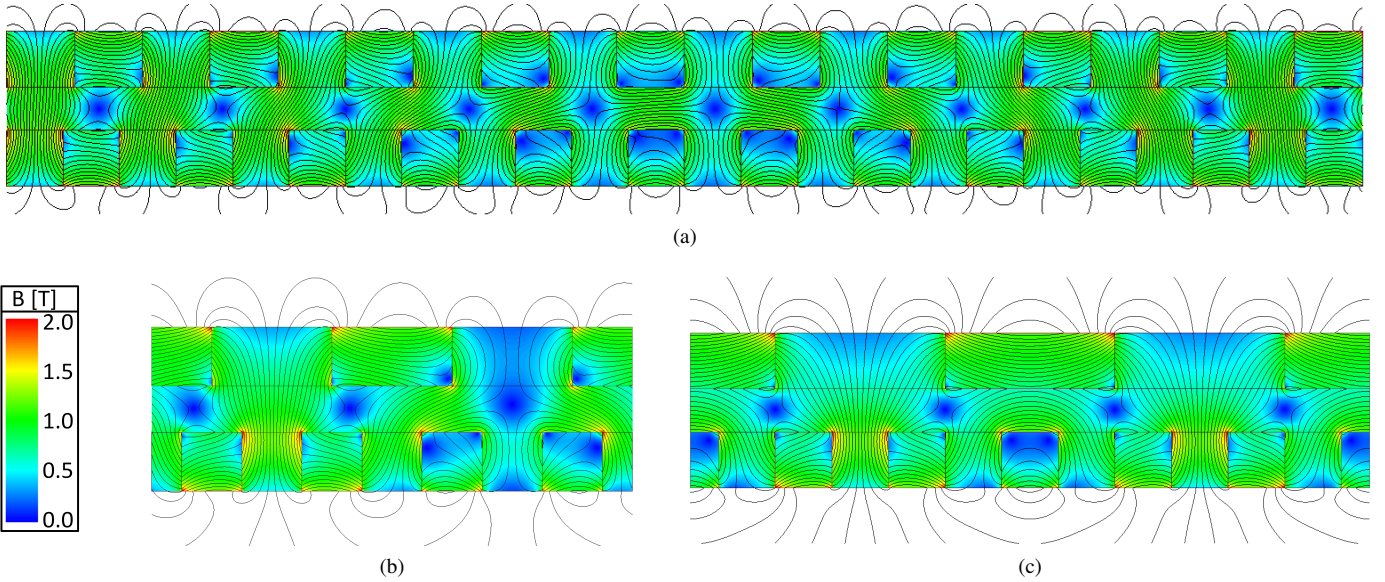


Fig. 7. Magnetic flux lines and density distributions of double-sided Halbach array rotors with the pole number combinations of (a) 36/30, (b) 36/18, and (c) 30/12. The plots show one circumferential periodicity, with matching boundary conditions applied. To enhance the clarity of the figure, the flux density values outside the airgaps and PMs, which are nearly zero, are not shown.

in Fig. 6, where the lower rotor has twice the pole number of the upper rotor.

The parameter k corresponds to the pole number ratio between the two rotors, defined as $k = \frac{P_1}{P_2}$. According to 4, the resultant flux density is the sum of two sine waves with different frequencies, where these frequencies are interconnected through the pole number ratio k . This ratio also influences the selection of the PM length for each rotor and the magnet-to-magnet gap. Therefore, the pole numbers must be chosen such that the flux density of each rotor positively interacts with the other, thereby enhancing the overall resultant flux density.

The flux line and density distributions for three combinations of pole numbers—36/30, 36/18, and 36/12—were calculated using 2D finite element analysis (FEA) and are shown in Fig. 7. These calculations were performed with matching boundary conditions and the smallest repeating unit for each combination. Different pole number combinations result in varying magnetic flux paths and distinct normal and tangential flux density components.

IV. THREE-DIMENSIONAL FINITE ELEMENT ANALYSIS

To further investigate the performance of the proposed concept, a combination of 36/18 pole numbers was selected, and a parametric 3D FEA model was developed using Ansys Electronics Desktop software [17]. Due to the circumferential symmetry, matching boundary conditions were applied over the $\frac{12\pi}{P_2} = \frac{24\pi}{P_1}$ section of the machine. In this example design,

the PM lengths of both rotors were assumed to be uniform, and the number of turns per coil for the stator associated with 18 poles was set to twice that of the other stator.

The open circuit induced voltages under two operational conditions were calculated and are plotted in Fig. 8. When the generator operates under normal conditions, as shown in Fig. 8a, there are two sets of two-phase voltages with different frequencies: one set corresponds to the 36-pole rotor and winding, and the other to the 18-pole rotor and winding. Besides the number of turns, the PM length of each rotor affects the flux density and induced voltage. For example, if the same voltage amplitude is required from both windings and mechanical limitations to prevent increasing the number of turns in stator 2, increasing the PM length of the 18-pole rotor can achieve the desired voltage.

The back EMF when only one rotor is active, and the other is non-operational due to a fault, such as PM demagnetization, is shown in Fig. 8b. In this scenario, the back EMF for the stator corresponding to the faulty rotor is zero, while the other stator continues to operate at its rated performance. This means the generator operates at exactly half of its rated power, allowing one of the outputs to still function at full load.

An essential criterion for a generator to be fault-tolerant is phase decoupling, which protects other phases from the fault of the other phase(s). In this study, a two-phase winding was employed for each stator because, in a two-phase winding, the

$$B_y = B_r \sum_{i=0}^{\infty} \frac{\sin(\epsilon n \pi / m)}{n \pi / m} \exp\left(\frac{-n \pi g_{M2M}}{2 \tau_{p1}}\right) \exp\left(\frac{-n \pi y}{\tau_{p1}}\right) \left\{ \left[1 - \exp\left(\frac{-n \pi L_{PM1}}{\tau_{p1}}\right) \right] \sin\left(\frac{n \pi (2x - (k-1) \tau_{p1})}{2 \tau_{p1}}\right) + \left[1 - \exp\left(\frac{-n \pi L_{PM2}}{k \tau_{p1}}\right) \right] \exp\left(\frac{-n \pi g_{M2M} (1-k)}{2 k \tau_{p1}}\right) \exp\left(\frac{n \pi y (1+k)}{k \tau_{p1}}\right) \sin\left(\frac{n \pi x}{k \tau_{p1}}\right) \right\} \quad (4)$$

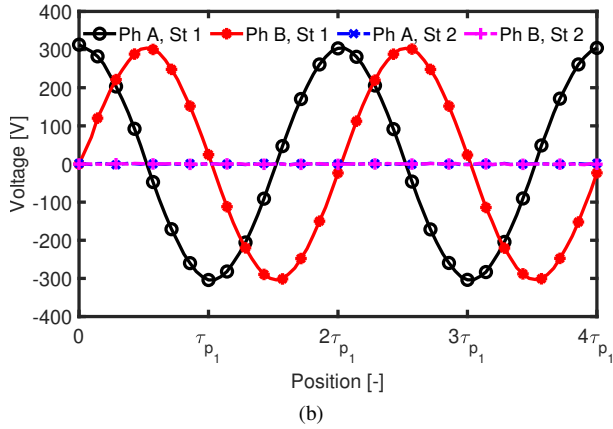
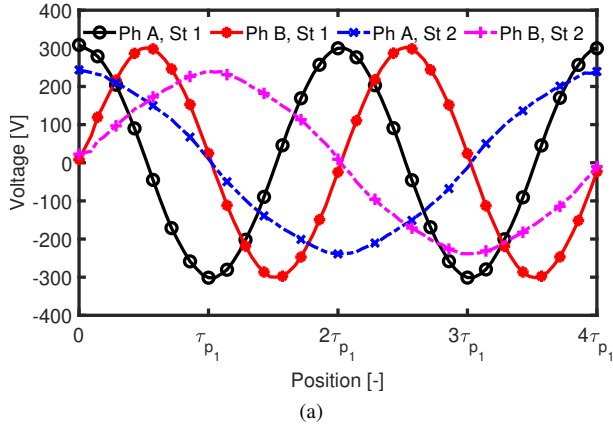


Fig. 8. The open circuit induced voltage when (a) both rotors are operational and (b) only one rotor is active.

phases of each stator are entirely decoupled, resulting in zero mutual inductance. However, the mutual inductance between the phases of different stators may still be present.

For the example generator under study with 36/18 rotor poles, the self and mutual inductances were calculated, and the results are presented in Fig. 9. The mutual inductance between the phases of different stators is zero, indicating no coupling between the stators. However, it should be noted that the mutual inductance between phases of different stators depends on the pole number difference between the two rotors and the stator topology. For this example, with the stator configuration set such that $\tau_c = \frac{3}{2}\tau_p$, the mutual inductances are zero. This may not be the case for other pole counts and stator topologies.

V. DISCUSSION

The proposed coreless AFPM generator with a double-sided Halbach array rotor, featuring different polarities on each side, allows for a single mechanical and cooling structure for both stators. This contrasts with the first and second topologies, which each have two separate electromagnetic units (see Figs. 1 and 2).

The integrated mechanical and cooling structure reduces the overall mass and volume of the system. An example cooling structure is shown in Fig. 10, where both stators are immersed in a coolant. This cooling configuration is inspired by [18, 19]

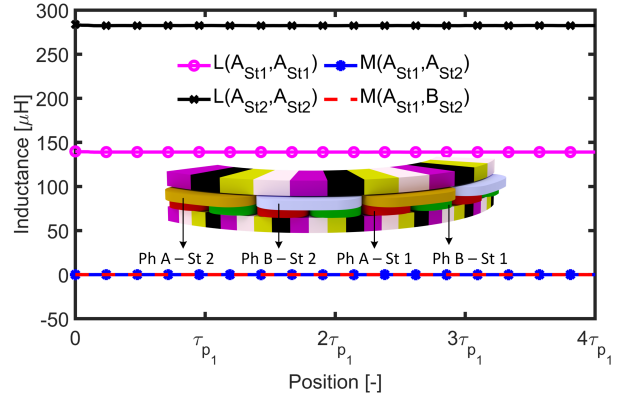


Fig. 9. Calculated self and mutual inductances using 3D FEA, illustrating zero phase coupling between phases of different and the same stator.

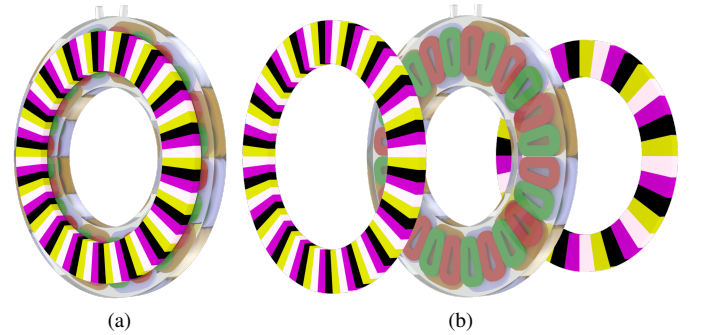


Fig. 10. Integrated cooling and mechanical concepts for both stators, facilitated by the shared air gap in a coreless AFPM generator topology with different polarity Halbach array rotors on each side, showing (a) compact and (b) exploded views.

that proposed stator immersion in coolant for yokeless and segmented armature (YASA) AFPM machines.

In coreless stator AFPM machines, the absence of stator teeth allows the stator windings to be directly exposed to the rotating magnetic flux generated by the PMs. This direct exposure induces alternating eddy currents in the stator conductors, resulting in energy losses. There are both tangential and normal components of magnetic flux density in the airgap, in which the normal component induces eddy currents across the width of the conductor, while the tangential component induces eddy currents along the depth of the conductor [20].

The total eddy current losses in conductors with a rectangular cross-section can be determined as [21]:

$$P_{ed} = \frac{\pi^2 N_c N_t f^2 t_w t_h l_c}{6\rho} (t_w^2 B_z^2 + t_h^2 B_\phi^2), \quad (5)$$

where, N_c represents the number of coil sides with an average length l_c , while N_t denotes the turns per coil. B_z and B_ϕ refer to the axial and tangential components of the flux density, respectively. t_w signifies the trace width, t_h denotes the trace height in the y-direction, and f indicates the frequency. This relationship highlights that the eddy current losses increase proportionally with the cube of the trace width, underscoring

the importance of minimizing trace width to mitigate high eddy current losses.

Rotors with varying pole numbers on each side exhibit higher tangential flux density compared to those with uniform polarity on both sides. This leads to increased eddy current losses, requiring a more precise and careful stator design for the proposed concept. To mitigate eddy current losses, narrower conductors and parallel paths can be used. Additionally, fine transposition of conductors is essential to prevent circulating losses within the parallel paths.

VI. CONCLUSIONS

This paper presents a multi-winding coreless AFPM generator with double-sided Halbach array rotors of different polarities. The proposed electromagnetic configuration features high power density, due to different windings sharing a single airgap, resulting in integrated mechanical and thermal structures. Additionally, it requires only one prime mover, reducing the overall system volume and mass. Analytical equations highlight the critical importance of selecting the appropriate pole number ratio for rotors on the resulting flux density in the airgap. Two-phase windings were employed to maximize decoupling between phases, and it was also demonstrated that proper pole number ratio selection could magnetically isolate multiple winding sets from each other.

ACKNOWLEDGMENT

The support of the Leverhulme Trust under their visiting professorship scheme, and of ANSYS Inc. and University of Kentucky the L. Stanley Pigman Chair in Power endowment is gratefully acknowledged. Any opinions, findings, and conclusions or recommendations expressed in this material are those of the authors and do not necessarily reflect the views of the sponsoring organizations.

REFERENCES

- [1] J. F. Eastham, B. Yin, X. Zeng, C. Hodge, and X. Pei, "Permanent magnet excitation of a two and four pole pair dual wound machine," in *Conference Proceedings of INEC*, 2022.
- [2] B. Yin, X. Pei, X. Zeng, J. F. Eastham, C. Hodge, and O. Simmonds, "Design and analysis of dual wound machine for electric ships," in *2020 International Conference on Electrical Machines (ICEM)*, vol. 1. IEEE, 2020, pp. 104–110.
- [3] T. Yazdan, M. Humza, and H.-W. Cho, "Three-phase dual-winding multitasked pmsm machine using double layer concentrated winding for hev application," *IEEE Access*, vol. 11, pp. 36 682–36 691, 2023.
- [4] B. Yin, X. Pei, J. F. Eastham, H. Wang, C. Hodge, O. Simmonds, C. Vagg, and X. Zeng, "Magnetic decoupling of winding design in dual wound generators," *IEEE Transactions on Energy Conversion*, vol. 38, no. 1, pp. 250–261, 2022.
- [5] J. F. Gieras, R.-J. Wang, and M. J. Kamper, *Axial flux permanent magnet brushless machines*. Springer Science & Business Media, 2008.
- [6] F. Nishanth, J. Van Verdegheem, and E. L. Severson, "A review of axial flux permanent magnet machine technology," *IEEE Transactions on Industry Applications*, vol. 59, no. 4, pp. 3920–3933, 2023.
- [7] F. Marcolini, G. De Donato, F. G. Capponi, M. Incurvati, and F. Caricchi, "Novel multiphysics design methodology for coreless axial flux permanent magnet machines," *IEEE Transactions on Industry Applications*, 2023.
- [8] S. Neethu, S. P. Nikam, S. Pal, A. K. Wankhede, and B. G. Fernandes, "Performance comparison between pcb-stator and laminated-core-stator-based designs of axial flux permanent magnet motors for high-speed low-power applications," *IEEE Transactions on Industrial Electronics*, vol. 67, no. 7, pp. 5269–5277, 2019.
- [9] M. J. Kamper, R.-J. Wang, and F. G. Rossouw, "Analysis and performance of axial flux permanent-magnet machine with air-cored nonoverlapping concentrated stator windings," *IEEE Transactions on Industry Applications*, vol. 44, no. 5, pp. 1495–1504, 2008.
- [10] F. Marignetti, G. Volpe, S. M. Mirimani, and C. Cecati, "Electromagnetic design and modeling of a two-phase axial-flux printed circuit board motor," *IEEE Transactions on Industrial Electronics*, vol. 65, no. 1, pp. 67–76, 2017.
- [11] F. Marcolini, G. De Donato, F. G. Capponi, M. Incurvati, and F. Caricchi, "On winding manufacturing technologies for coreless axial-flux permanent-magnet machines," in *2023 IEEE Workshop on Electrical Machines Design, Control and Diagnosis (WEMDCD)*. IEEE, 2023, pp. 1–7.
- [12] Y. Chulaee, D. Lewis, M. Vatani, J. F. Eastham, and D. M. Ionel, "Torque and power capabilities of coreless axial flux machines with surface pms and halbach array rotors," in *2023 IEEE International Electric Machines & Drives Conference (IEMDC)*. IEEE, 2023, pp. 1–6.
- [13] M. Vatani, Y. Chulaee, A. Mohammadi, D. R. Stewart, J. F. Eastham, and D. M. Ionel, "On the optimal design of coreless afpm machines with halbach array rotors for electric aircraft propulsion," in *2024 IEEE Transportation Electrification Conference & Expo (ITEC)*. IEEE, 2024.
- [14] M. Vatani, A. Mohammadi, D. Lewis, J. F. Eastham, and D. M. Ionel, "Coreless axial flux halbach array permanent magnet generator concept for direct-drive wind turbine," in *2023 12th International Conference on Renewable Energy Research and Applications (ICRERA)*. IEEE, 2023, pp. 612–617.
- [15] K. Halbach, "Physical and optical properties of rare earth cobalt magnets," *Nuclear Instruments and Methods in Physics Research*, vol. 187, no. 1, pp. 109–117, 1981.
- [16] G. Ramian, L. Elias, and I. Kimel, "Micro-undulator FELS," *Nuclear Instruments and Methods in Physics Research Section A: Accelerators, Spectrometers, Detectors and Associated Equipment*, vol. 250, no. 1-2, pp. 125–133, 1986.
- [17] *Ansysis® Electronics, Maxwell, version 23.1, 2023, ANSYS Inc.*
- [18] R. Camilleri, P. Beard, D. A. Howey, and M. D. McCulloch, "Prediction and measurement of the heat transfer coefficient in a direct oil-cooled electrical machine with segmented stator," *IEEE Transactions on Industrial Electronics*, vol. 65, no. 1, pp. 94–102, 2017.
- [19] R. Camilleri and M. D. McCulloch, "Integrating a heat sink into concentrated wound coils to improve the current density of an axial flux, direct liquid cooled electrical machine with segmented stator," *Energies*, vol. 14, no. 12, p. 3619, 2021.
- [20] R.-J. Wang and M. J. Kamper, "Calculation of eddy current loss in axial field permanent-magnet machine with coreless stator," *IEEE Transactions on Energy Conversion*, vol. 19, no. 3, pp. 532–538, 2004.
- [21] N. Taran, D. M. Ionel, V. Rallabandi, G. Heins, and D. Patterson, "An overview of methods and a new three-dimensional FEA and analytical hybrid technique for calculating ac winding losses in pm machines," *IEEE Transactions on Industry Applications*, vol. 57, no. 1, pp. 352–362, 2021.